AD-A140 659 STUDY OF THE INFLUENCE OF METALLURGICAL FACTORS ON FATIGUE AND FRACTURE O..(U) SOUTHWEST RESEARCH INST SAN ANTONIO TX J LANKFORD ET AL. FEB 84 SWRI-06-7436 1/1

UNCLASSIFIED AFOSR-TR-84-0253 F49620-83-C-0054 F/G 11/6 NL

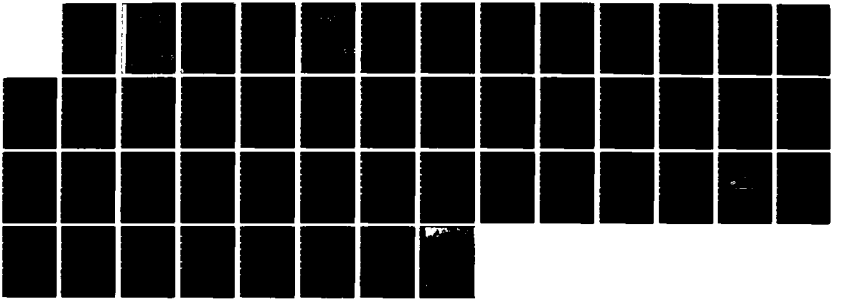

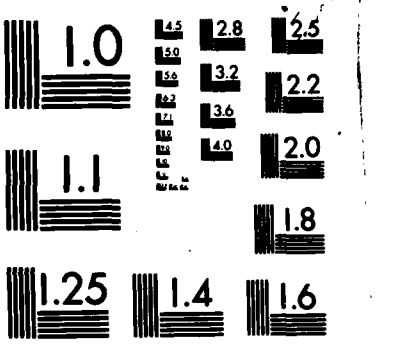

MICROCOPY RESOLUTION TEST CHART
NATIONAL BUREAU OF STANDARDS-1963-A

SwRI-7436

(3)

STUDY OF THE INFLUENCE OF METALLURGICAL FACTORS ON FATIGUE AND FRACTURE OF AEROSPACE STRUCTURAL MATERIALS

by
James Lankford
David L. Davidson
Gerald R. Leverant
John E. Hack

AFOSR ANNUAL REPORT

This research was sponsored by the Air Force Office of Scientific Research,
Electronic and Materials Sciences Directorate
Under Contract F49620-83-C-0054

Approved for release; distribution unlimited.

PUBLIC

February 1984

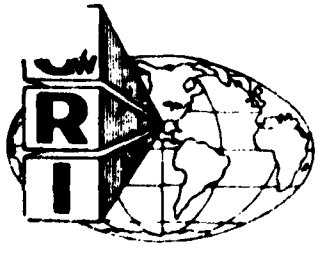

SOUTHWEST RESEARCH INSTITUTE
SAN ANTONIO HOUSTON

UNCLASSIFIED

SECURITY CLASSIFICATION OF THIS PAGE (When Data Entered)

REPORT DOCUMENTATION PAGE	READ INSTRUCTIONS BEFORE COMPLETING FORM
1. REPORT NUMBER: AFOSR-TR- 84-0253	2. GOVT ACCESSION NO.: AD-A140 659
	3. RECIPIENT'S CATALOG NUMBER:
4. TITLE (and Subtitle): Study of the Influence of Metallurgical Factors on Fatigue and Fracture of Aerospace Structural Materials	5. TYPE OF REPORT & PERIOD COVERED: Annual Scientific Report 1 Jan 1983 - 31 Dec 1983
	6. PERFORMING ORG. REPORT NUMBER: 06-7436
7. AUTHOR(s): James Lankford, David L. Davidson, Gerald R. Leverant, John E. Hack	8. CONTRACT OR GRANT NUMBER(s): F49620-83-C-0054
9. PERFORMING ORGANIZATION NAME AND ADDRESS: Southwest Research Institute, 6220 Culebra Road (P.O. Drawer 28510), San Antonio, TX 78284	10. PROGRAM ELEMENT, PROJECT, TASK AREA & WORK UNIT NUMBERS: 61102F, 2306/A1
11. CONTROLLING OFFICE NAME AND ADDRESS: AF Office of Scientific Research/NE, Bolling AFB, Building 410, Washington, DC 20332	12. REPORT DATE: February 1984
	13. NUMBER OF PAGES: 44
14. MONITORING AGENCY NAME & ADDRESS (if different from Controlling Office)	15. SECURITY CLASS. (of this report): UNCLASSIFIED
	15a. DECLASSIFICATION/DOWNGRADING SCHEDULE

16. DISTRIBUTION STATEMENT (of this Report)

Approved for public release; distribution unlimited

17. DISTRIBUTION STATEMENT (of the abstract entered in Block 20, if different from Report)

18. SUPPLEMENTARY NOTES

19. KEY WORDS (Continue on reverse side if necessary and identify by block number)

Fatigue	Titanium Alloys
Fracture	Single Crystals
Crack Growth	Crack Tip Plasticity
Nickel-Base Superalloys	Crack Growth Modeling
Aluminum Alloys	Crystallographic Orientation

20. ABSTRACT (Continue on reverse side if necessary and identify by block number)

This report summarizes the results of a two-phase study involving (1) experimental characterization and analytical modeling of fatigue crack tip micromechanics in aerospace structural (Al and Ti) alloys, and (2) identification and modeling of key factors controlling subcritical crack growth and unstable fracture in single crystal nickel-base superalloys.

In the micromechanics phase of the program, fatigue crack growth at near-threshold rates has been modeled using concepts previously suggested by

DD FORM 1 JAN 73 1473

UNCLASSIFIED

SECURITY CLASSIFICATION OF THIS PAGE (When Data Entered)

TR-84-0253

Hornbogen and Zum Gar, Neumann and others. Crack tip opening displacement, the increment of crack advance, and crack tip strain are assumed to be dependent on the formation of slip lines at the crack tip. Slip line length and dislocation density are parameters in the model which are controlled by the microstructure. These concepts are used together with crack tip plasticity and crack growth information recently derived by Davidson and Lankford for aluminum alloys. The model may be used in two ways: to predict the increment of crack growth, if the slip line length is known, or the length of the slip line may be determined if the crack growth increment is measured. Crack tip plasticity data for 7075-T651 is used to evaluate the model, and the results obtained are compatible with the assumptions, and give a value of slip line length which is compatible with the mean free slip length in the material.

In the single crystal nickel-base superalloy task, the details of anisotropic fracture mechanics and crack tip stress field solutions have been reviewed. The concepts derived have been used to establish a test matrix for the determination of the influence of crystallographic orientation and applied stress state on crack tip deformation and crack growth behavior. Both uniaxial tests on compact tension specimens and multiaxial tests on notched tubes are currently being conducted. Initial results indicate a significant effect of the ratio of applied shear stress to applied normal stress on crack growth rate in the multiaxial tests. A heat treatment for modifying the γ' distribution, and thus the slip character, has also been identified.

AFOSR-TR- 84-0253

SOUTHWEST RESEARCH INSTITUTE
Post Office Drawer 28510, 6220 Culebra Road
San Antonio, Texas 78284

STUDY OF THE INFLUENCE OF METALLURGICAL FACTORS ON FATIGUE AND FRACTURE OF AEROSPACE STRUCTURAL MATERIALS

by
James Lankford
David L. Davidson
Gerald R. Leverant
John E. Hack

AFOSR ANNUAL REPORT

This research was sponsored by the Air Force Office of Scientific Research,
Electronic and Materials Sciences Directorate
Under Contract F49620-83-C-0054

Approved for release; distribution unlimited.

PUBLIC

February 1984

Approved:

U. S. Lindholm, Director
Department of Materials Sciences

TABLE OF CONTENTS

TABLE OF CONTENTS (CONTINUED)

LIST OF FIGURES

LIST OF TABLES

I. RESEARCH OBJECTIVES

A. Task 1. Influence of Metallurgical Structure Upon Crack Tip Micromechanics

1. Define experimentally the physical basis and extent of crack advance in alloys of varying, well-characterized microstructure.

2. Determine and measure experimentally the microstructural and micromechanical elements which control subcritical crack advance.

3. Incorporate microstructural and crack tip micromechanical parameters into a fundamental crack growth model.

B. Task 2. Fracture Mechanisms in Single Crystal Nickel-Base Superalloys

1. Determine the influence of crystallographic orientation on subcritical crack growth and unstable fracture.

2. Identify the relative importance of shear and normal stresses on slip band cracking.

3. Define the role of slip character on subcritical crack growth and unstable fracture.

4. Develop a model for prediction of fracture behavior.

II. STATUS OF THE RESEARCH EFFORT

A. Task 1. Influence of Metallurgical Structure Upon Crack Tip Micromechanics

1. Scope

The intensive effort of the past several years to measure crack tip parameters (strains, CTOD, etc.) has provided extensive information on several alloy systems. This year the focus of effort was extended to incorporate this information into micromechanical models for fatigue crack growth. Preliminary experimental work was also begun on defining the crack tip mechanics of a family of high temperature powder metallurgy alloys. The overall thrust of the present work is to understand and model the effect of metallurgical and microstructural factors on the micromechanics of fatigue crack extension in aluminum and titanium alloys.

2. A Model for Fatigue Crack Advance Based on Crack Tip Metallurgical and Mechanics Parameters

Fatigue crack growth at near-threshold rates has been modeled using concepts previously suggested by Hornbogen and Zum Gar, Neumann and others. Crack tip opening displacement, the increment of crack advance, and crack tip strain are assumed to be dependent on the formation of slip lines at the crack tip. Slip line length and dislocation density are parameters in the model which are controlled by the microstructure. These concepts are used together with crack tip plasticity and crack growth information recently derived by Davidson and Lankford for aluminum alloys. The model may be used in two ways: to predict the increment of crack growth, if the slip line length is known, or the length of the slip line may be determined if the crack growth increment is measured. Crack tip plasticity data for 7075-T651 is used to evaluate the model, and the results obtained are compatible with the assumptions, and give a value of slip line length which is compatible with the mean free slip length in the material.

a. Introduction

Fatigue crack growth rate is known to depend upon a number of metallurgical factors. Hornbogen and Zum Gar developed a qualitative model for a precipitation hardened [1] alloy of Fe-Ni-Al, which included

1) the effect of precipitate shearability on slip reversibility and homogeneity; and

2) the effect of slip localization within a single grain.

Later, Lindigkeit, Terlinde, Gysler and Lutjering used this model to examine their results for Al-Zn-Mg-Cu [2] and Ti-Al alloys [3]. A more

quantitative model using slip length and dislocation pileup theory was recently formulated by Terlinde and Lutjering for tensile fracture in Ti-Al alloys of varying grain size [4].

Using a completely different approach, Chakrabortty has formulated a model for fatigue crack growth, but which also used slip length [5]. This model was the latest and most refined of a series of similar models initiated by Liu and Ino [6] in 1969. A similar series of models, built on the original work of McClintock and Irwin in 1965, was recently articulated in its most advanced form by Lanteigne and Bailon [7]. These models do not explicitly define a slip length, but instead use the concept of a process zone, defined as a region in which metallurgical factors are important. Saxena and Antolovich [8] determined that the size of the "process zone" correlated with subcell size for Cu and Cu-2.2Al and with the grain size for Cu-6.3Al, which did not readily form subcells. In modeling the growth of small fatigue cracks, Tanaka [9] has also used the concept of a grain size limited slip line, and modeled the process using the BCS theory. Experimental work on very rapidly growing fatigue cracks, observed under high resolution conditions by Neumann [10] and Vehoff and Neumann [11], have shown the detailed steps accompanying crack extension and supplied some information on the formation of slip lines at the crack tip. Although microstructural parameters are not included in their analysis, crystallographic factors are.

The efforts of these numerous investigators to relate microstructural parameters to the macroscopic factors driving fatigue crack growth has been hampered by the necessity of having to use either theoretical determinations or assumptions about the behavior of the crack tip. Recent dynamic observations of fatigue crack growth under high resolution conditions coupled with accurate determinations of crack tip opening displacements and strains have provided information not previously available. Interpretation of results from this work [12], have led to the conclusion that failure of the material at the crack tip can be described in the same way as failure of a low-cycle fatigue specimen. Thus, ΔN cycles are required for the sudden advance of the crack by an increment Δa. This finding has substantiated a major assumption of all the models previously mentioned except that of Neumann. There still remains, however, the necessity to relate microstructural parameters to Δa; the purpose of this paper is to present a model to tie microstructural parameters to the external forces driving the crack.

The model will use many of the same ideas previously presented, but formulates the relations in a new way and incorporates the empirical relationships we have previously determined. The results of the model are examined using previously published data on 7075-T651 aluminum alloy [12,13].

Findings from that work which are considered to be important to crack growth, and which will be included in the model, are listed below:

1. Both crack tip opening displacement (CTOD) and crack tip strain generally increase with increasing cyclic stress intensity factor (ΔK), but a range of values for both is found at any one ΔK.

2. Striation spacing is considered to be a measure of the increment of crack growth, which for cracks grown without environmental influence, does not correlate with either CTOD or crack growth rate.

3. All measured crack tip parameters may be correlated with ΔK in the range studied. This considers similitude to exist between crack tip fields for various lengths of crack.

b. The Model

At very low growth rates when ΔK just exceeds the threshold value ΔK_{TH}, crack tip slip line geometry is considered to be as shown in Figure 1. Following the ideas of Hornbogen and Zum Gar, one slip line having n_o dislocations is caused by loading such a fatigue crack tip. On the unloading portion of the cycle, n_R dislocations move back along the slip line to the crack tip. The total slip offset on this one cycle therefore

$$(n_o - n_R)b \qquad (1)$$

The length of the slip line r_s could be related to a number of parameters, which might include the mean free dispersoid spacing, the coherency of the precipitates and the dispersoids, the grain size, the shear stress τ exerted on the slip plane, details of the crystallography and favorable slip plane geometry, and the degree to which secondary slip systems are activated.

On succeeding cycles, it is probable that an increasing difference will occur between the number of dislocations generated at the crack tip on the loading cycle and the number which return on the unloading cycle. With each cycle, some debris is likely to collect along the slip plane, due to the threading of that plane by dislocations from activated secondary sources and imperfect reverse slip. This causes an increase in the difference $(n_o - n_R)$ on succeeding cycles, which lowers the effective driving stress by shielding the crack tip. Conversely, continued shearing of precipitate particles by the shuttling dislocations could work soften the material by reversion or "scrambling" of the precipitates. Work softening appears to be partially controlled by the dispersoid distribution, so that in commercial aluminum alloys it is less likely than work hardening [14]. The slip distance r_s may also change with increasing cycles; it could either increase or decrease depending on the slip character of the material.

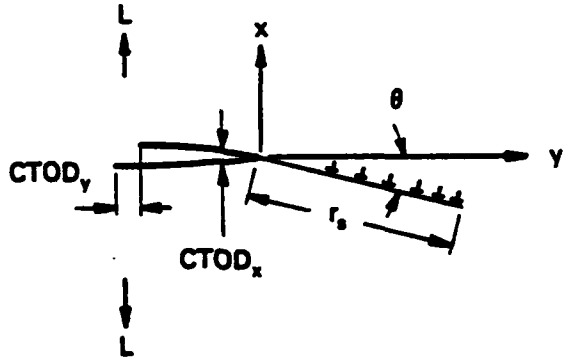

FIGURE 1. CRACK AT A ΔK_{eff} JUST EXCEEDING THRESHOLD. The crack has one slip plane coming from the crack tip at an angle θ to the growth direction. On the slip plane are D_N dislocations.

Dynamic observation of fatigue crack growth in these alloys has shown that the crack begins a sequence leading to crack growth as a sharp crack tip (small CTOD), and blunts on succeeding cycles (increasing CTOD). The details of this process are not known, and are probably not the same for each growth increment. Likewise, the changes in n_O and n_R with number of cycles is complex, with the details not now known. Thus, for the following model $D_N = (n_O - n_R)$ will be considered to be a typical equilibrium value after some cyclic deformation at the crack tip has occurred. Therefore, the model is not for any one cycle, but relates to an average value.

The model to be developed pertains only to the crack tip and the material immediately adjacent. Farther out in the plastic zone slip also occurs causing strain, but these slip lines are considered to be only indirectly related to the slip lines at the crack tip. For the condition shown in Figure 1, crack opening displacement parallel to x, the loading axis, becomes

$$CTOD_x = D_N b \sin \theta \tag{2}$$

and the increment of crack advance along the slip line is

$$\Delta a = D_N b \tag{3}$$

The condition described above is for a crack slightly above the threshold for growth. At higher growth rates, the crack tip is considered to deform by emitting a number of slip lines N(K) at an angle θ to the line of the crack. The crack tip is geometrically modeled as illustrated in Figure 2. The experimental work of Neumann [10] indicates that this general geometric condition definitely pertains at high crack growth rates. His photographs show numerous slip lines emanating from the crack tip.

Using the crack tip geometry shown in Figure 2,

$$CTOD_x = N(K)\ D_N b \sin \theta \tag{4}$$

and the crack growth increment, taken on average perpendicular to the loading, is

$$\Delta a = N(K)\ D_N b \cos \theta \tag{5}$$

The length of the slip lines r_s, the number of dislocations on the slip plane D_N and the stress are all related for both of these cases by the mathematics describing a single pileup of dislocations under stress. The relation derived by Hirth and Lothe [15] for this case is

$$D_N b = \frac{\pi(1-\nu)}{\mu} \tau\ r_s \tag{6}$$

where ν = Poissons ratio, μ = shear modulus, and τ = shear stress on the slip plane.

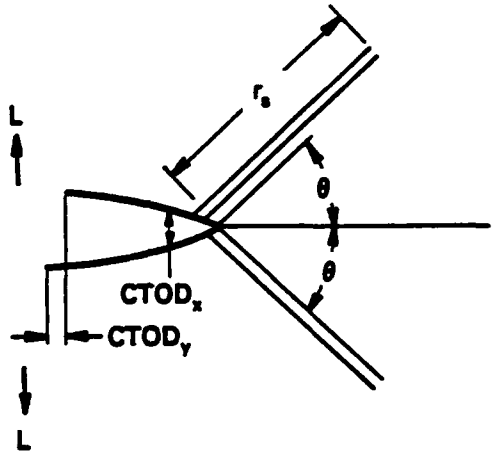

FIGURE 2. CRACK AT LARGE ΔK_{eff}, SHOWING 4.5 SLIP LINES AT THE ANGLE θ TO THE DIRECTION OF CRACK GROWTH. Slip lines are assumed to be separated by the distance $D_N b$.

Shear stress at the crack tip has been determined by Davidson and Lankford for low-carbon steel [16] through the size of the subgrains which form during fatigue crack growth. We have also determined the crack tip shear strain for this material [16], and computed the same values of shear stress using the cyclic stress-strain curve

$$\Delta\tau = K_1 \left(\frac{\Delta\gamma_p}{2}\right)^{n'} \tag{7}$$

Thus, it is assumed that the cyclic stress-strain curve measured for aluminum alloys also allows stresses to be computed from measured strains, as it has for low-carbon steel. This allows Eq. (6) to be rewritten in terms of the plastic shear strain range $\Delta\gamma_p$.

$$D_N b = \frac{\pi(1-\nu)K_1}{\mu} \left(\frac{\Delta\gamma_p}{2}\right)^{n'} r_s \tag{8}$$

The above formulation implies that stress computed from measured strain adequately describes the stress τ acting on the slip plane of the pileup. Strain, as determined from the pileup is not defined, nor is displacement, as related to the measured strain. Such definitions are a point of much difficulty in the formulation of models of this type, so the side-stepping of this issue is necessary. For all the models previously mentioned which require the use of stress or strain near the crack tip, no method which is more accurate than the one offered here has been suggested.

The analysis of fatigue cracks using the stereoimaging technique has allowed direct measurement of CTOD and computation from the measured displacements of the crack tip strains [12]. The three in-plane elements of the strain tensor, as well as the principal strains and maximum shear strain have been determined [12]. The plastic component of the maximum shear strain at the crack tip $\Delta\gamma_p$ is chosen here as the relevant value of strain. Detailed fractography has resulted in measurement of crack advance increment Δa [13]. These quantities have been averaged and correlated with the effective applied cyclic stress intensity factor $\Delta K_{eff} = \Delta K - \Delta K_{TH}$:

$$CTOD = C\Delta K_{eff}^{q} \tag{9}$$

$$\Delta\gamma_p = K_o \Delta K_{eff}^{r} \tag{10}$$

$$\Delta a = A_c \Delta K_{eff}^{n} \tag{11}$$

Combining Eqs. (2) and (9) gives, near ΔK_{TH},

$$C\Delta K_{eff}^{q} = D_N b \sin\theta \tag{12}$$

$D_N b$ may be determined by combining Eqs. (8) and (10)

$$D_N b = C_1 \, r_s \, \Delta K_{eff}^{n'r} \tag{13}$$

where C_1 combines all the constant values. Thus, $D_N b$ is expressed in terms of both the slip line length and the stress intensity factor, which makes it possible to insert the relevant metallurgical slip length controlling parameter for the alloy and compute the number of dislocations in the pile-up which will result at any stress intensity factor. By knowing $D_N b$, and using Eq. (12), the angle θ at ΔK_{TH} can be computed. The relation between these parameters may be visualized using the construction shown in Figure 3.

The model may be used in two ways, depending on whether Δa is to be computed or is known and used in the computation. First, we will examine the computation of Δa, assuming that the quantities in Eqs. (9) and (10) are known. To complete the model, it is necessary to assume a dependence of θ on ΔK. Since θ at ΔK_{TH} is determined, it is necessary to know θ at an upper limit and assume some $\theta(K)$ dependence in between. The strain analysis by Hutchinson [17] indicates that the value of θ for maximum shear strain occurs at approximately 85°, and this value has been taken for the model. The function $\theta(\Delta K)$ is assumed to be

$$\theta(K) = \theta_o \Delta K_{eff}^{u} \tag{14}$$

where θ_o and u may be determined from the ΔK_{TH} value of θ and the upper limit of θ at a high ΔK, which is a variable. It may be necessary to assume other functions for different materials.

Inputs for the model are:

1) Material parameters ν and μ and the cyclic stress-strain curve.

2) Slip plane length r_s, which is dependent on a microstructural factor limiting the length of the slip plane.

3) ΔK_{TH} and the empirically derived parameters C, q, K_o, and r in Eqs. (9) and (10).

4) The value of K at which $\theta = 85°$.

The model then allows computation of

1) θ, N(K) and the crack growth increment Δa.

2) $CTOD_y$, defined as the Mode II crack opening displacement.

Crack advance Δa occurs because of the permanent displacement $D_N b$ which accumulates by irreversible slip processes during ΔN cycles. It has been shown previously [12] that ΔN may be determined by considering

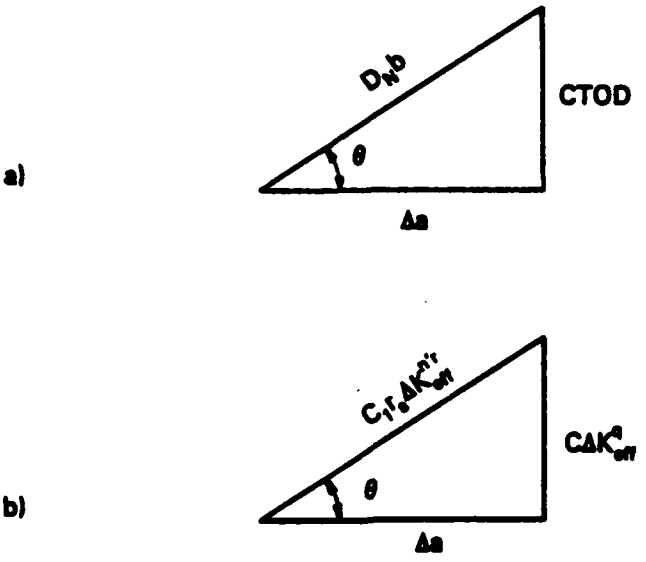

FIGURE 3. GEOMETRIC RELATIONS BETWEEN PARAMETERS MEASURED AND DERIVED BY THE MODEL, FOR NEAR ΔK_{TH} CONDITIONS.

a) In terms of the model parameters.

b) In terms of the measured material parameters. For higher ΔK, the hypotenuse is multiplied by N(K).

the fracturing element at the fatigue crack tip as similar to a low-cycle fatigue specimen; failure occurs according to the equation

$$\Delta\gamma_p \Delta N^{\beta} = \varepsilon_c \tag{15}$$

where ε_c and β were determined from the measured crack tip parameters, Eqs. (9)-(11).

Crack growth rate da/dN may then be computed from $\Delta a/\Delta N$. At near-threshold crack growth rates, Δa is caused by irreversibility along one slip band, which occurs slowly, over numerous cycles, because of the low crack tip stress; few secondary slip planes are activated which are the primary source of debris accumulation and which cause imperfections in reversibility. As ΔK increases, so does the rate of slip plane imperfection accumulation; thus, the number of cycles ΔN decreases.

The crack growth rate da/dN may be computed using Eqs. (5) and (15).

$$\frac{da}{dN} = \frac{\Delta a}{\Delta N} = \frac{N(K) D_N b \cos\theta}{\left(\frac{\varepsilon_c}{\Delta\gamma_p}\right)^{1/\beta}} \tag{16}$$

Substituting Eq. (13) for $D_N b$ and Eq. (10) for $\Delta\gamma_p$ gives

$$\frac{da}{dN} = \frac{N(K) C_1 \cos\theta \; r_s}{(\varepsilon_c/K_o)^{1/\beta}} \Delta K_{eff}^{(n'+1/\beta)r} \tag{17}$$

Empirically the crack growth rate may be expressed as

$$\frac{da}{dN} = B\Delta K_{eff}^{s} \tag{18}$$

Comparing Eqs. (17) and (18) gives

$$B = \frac{N(K) C_1 \cos\theta}{(\varepsilon_c/K_o)^{1/\beta}} \tag{19}$$

$$s = (n'+1/\beta)r \tag{20}$$

Solving Eq. (20) for β gives

$$\beta = \frac{r}{s - n'r} \tag{21}$$

Previously [12], β was derived from crack tip mechanics factors as

$$\beta = \frac{r}{s-n} \tag{22}$$

Comparison of Eqs. (21) and (22) gives the exponent in Eq. (11)

$$n = n'r \tag{23}$$

The constant A_o in Eq. (11) may be determined by combining Eqs. (4), (5), (8) and (9) to give

$$A_o = \frac{C}{\tan \theta} \Delta K^{q-n} \tag{24}$$

If Δa has been measured, and may be represented by Eq. (11) then the model may be used in a second way. Eqs. (2), (3) and (9) may be combined to give, near ΔK_{TH}

$$\theta = \text{Arc sin } (\frac{C}{A_o} \Delta K_{eff}^{q-n}) \tag{25}$$

Slip line length r_s is then determined from Eqs. (12) and (13). At higher ΔK_{eff}, Eqs. (8) and (10) are combined to compute $D_N b$, and Eqs. (4) and (5) are combined to give

$$\theta = \text{Arc tan } (\frac{C}{A_o} \Delta K_{eff}^{q-n}) \tag{26}$$

Eq. (4) or (5) is then used to compute N(K).

c. Evaluation of the Model

Data obtained from the ingot-derived, peak-aged aluminum alloy 7075-T651 will be used to evaluate the model [12]. Cracks were grown in vacuum (or a very dry environment) over the range $6 < \Delta K < 12$ MN/m$^{3/2}$, and the crack tip parameters listed in Table I were measured.

Equations (2)-(26) were incorporated into minicomputer programs which had as their input and output those values previously given. Table II shows values for the various parameters computed by using the model in the second way described; i.e., θ is computed from measured Δa and CTOD. Conversely, if the model is used in the first way described, with r_s and $\theta(K)$ as inputs, the results of Table III are obtained. Using the model in this way requires $\Delta K(\theta = 85°)$ be chosen; 12 MN/m$^{3/2}$ was used in the computation of Table III.

The computation of $CTOD_y$ (Row 7 of Tables II and III) is made by using the expression

$$CTOD_y = N(K_o) D_N b \cos \theta \tag{27}$$

TABLE I

CRACK TIP PARAMETERS
7075-T651 in a Vacuum/Dry Environment

ΔK = $MN/m^{3/2}$ CTOD and Δa = m

$C = 1.4 \times 10^{-10}$	K_1 = 775 MPa
q = 3.6	n′ = .0594
$K_o = 1.3 \times 10^{-4}$	$\mu = 2.6 \times 10^4$ MPa
r = 3.0	ν = 0.33
$A_o = 2 \times 10^{-7}$	β = 0.49
n = 0.27	ε_c = 0.4

TABLE II

7075-T651 VACUUM
r_s = 8.8 μm

ΔK MN/m$^{3/2}$	4	6	8	10	15
θ(°)	4	15.3	35.5	56	80
N(K)	1	1.1	1.3	2	6.6
$D_N b$	0.29	0.31	0.33	0.34	0.37
D_N	972	1044	1100	1144	1230
$CTOD_x$	0.021	0.089	0.25	0.56	2.4
$CTOD_y$	0.29	0.03	0.08	0	0.04
Δa	0.29	0.32	0.35	0.37	0.42

$D_N b$, CTOD and Δa = μm.

TABLE III

7075-T651 VACUUM
r_s = 8.8 μm

ΔK MN/m$^{3/2}$	4	6	8	10	15
θ(°)	4	12.5	27.7	51.3	85
N(K)	1	1.3	1.6	2.1	6.5
$D_N b$	0.29	0.31	0.33	0.34	0.37
D_N	970	1041	1096	1140	1225
$CTOD_x$	0.021	0.089	0.25	0.56	2.4
$CTOD_y$	0.29	0.09	0.12	0.02	0.02
Δa	0.29	0.40	0.47	0.46	0.21

$D_N b$, CTOD and Δa = μm.

where $N(K_o)$ = the non-symmetrical magnitude of N(K), which is determined as follows: at $\Delta K = 8$ MN/m$^{3/2}$, the value of N(K) = 1.3, but for symmetric yielding, N(K) = 2. Therefore, the non-symmetric magnitude of N(K) is the difference, 0.7.

Comparison of the values of Δa computed in Table III with those measured (Table II) indicates that a reasonable value can be computed using the model, if r_s and $\Delta K(\theta = 85°)$ are properly chosen, except at ΔK = 15 MN/m$^{3/2}$. The values of θ and N(K) are computed assuming that threshold ΔK is slightly lower than 4 MN/m$^{3/2}$. Crack growth rates for the material tested [12] did not indicate an ever more rapidly decreasing rate with decreasing ΔK, which would have allowed deduction of a threshold ΔK, but rather remained linear down below 6 MN/m$^{3/2}$. Thus, the parameters in Table I were derived on the basis that $\Delta K_{TH} = 0$ because both CTOD and $\Delta\gamma_p$ correlated best with ΔK when this assumption was made. The crack growth data of Kirby and Beevers [18] indicates that $\Delta K_{TH} \simeq 3.5$ MN/m$^{3/2}$ is very near threshold and conforms to the assumption of the model.

The crack growth rate parameters B and s may be computed from Eqs. (19) and (20) using the values listed in Tables I and II (Table IV). Likewise, the crack growth increment parameters n and A_o may be computed from Eqs. (23) and (24). The computed value of n = 0.18, which is lower than the 0.27 measured; consequently it is not surprising that A_o is not a constant value, but varies with ΔK.

TABLE IV

COMPARISON OF MEASURED AND COMPUTED VALUES OF CRACK GROWTH RATE PARAMETERS

	Computed	Measured
B	1.2×10^{-14}	1.6×10^{-14}
s	6.4	6.3

d. Discussion

The model presented greatly simplifies the actual conditions at the crack tip; however, the resulting assumptions allow connection of the material microstructure with CTOD, crack growth increment and crack tip strain. Use of the model with average data from 7075-T651 indicates that these parameters can be quantified with a crack tip having less than 2 slip lines for $\Delta K < 10$ MN/m$^{3/2}$ but with a rapid increase for higher ΔK. The derived angles fit well with those observed and determined theoretically. This model predicts that there should exist a Mode II crack opening, $CTOD_y$,

which has been observed [19], and the trend and magnitude of the predicted change in $CTOD_y$ are similar to observations, in that $CTOD_y$ (at 1 μm behind the crack tip) is approximately equal to $CTOD_x$ for $\Delta K = 6$ MN/m$^{3/2}$, but decreases relative to $CTOD_x$ as ΔK increases. Crack tip geometry, as listed in Table II, is drawn approximately to scale in Figure 4. The predicted number of dislocations per slip plane appears to be reasonable, being spaced each 12b on the average at $\Delta K = 15$ MN/m$^{3/2}$, which is the highest density. This condition is relatively insensitive to the assumptions. The value of $r_s = 8.8$ μm derived for 7075-T651 is rather insensitive to the values of the crack tip constants found in Table I, but it is sensitive to the magnitude of the cyclic stress-strain curve K_1, as is shown in Table V.

The most probable values of K_1 are $700 < K_1 < 900$ MPa, which would mean $7 < r_s < 10$ μm. These values of r_s should be related to the microstructure in some way. Unfortunately, no one has derived a method for measuring this parameter for this material [20], unlike some titanium alloys where a value of r_s may be more readily derived from the microstructure. For 7075-T651, the dispersoid spacing as derived from transmission electron microscopy is in the range 0.5-2 μm [21], and the grain size is about 200 μm. Thus the derived value of r_s is in the size range of the dispersoid spacing, as would be reasonable for this alloy; r_s might also be related to the mean free path, MFP, in this material, which is greater than dispersoid spacing. MFP is defined as the average distance along a straight line between dispersoids. MFP is related to the diameter (d) and volume fraction of dispersoids (f) by [22]

$$MFP = \frac{2}{3} d(1-f)/f \tag{28}$$

For 7075-T651, f = 1-2% [23] which means $3.3 < MFP < 6.6$ μm. If the average value of 5 μm is used as the slip distance r_s, along with $K(\theta = 85°) = 13$ MN/m$^{3/2}$ and $K_1 = 825$ MN/m^2, the results in Table VI are derived using the model.

As may be judged from the ratio of computed Δa to striation spacing (ss) derived from fractography--the last row of Table VI--the agreement is satisfactory. Thus, it is concluded that the parameters in the model may be changed slightly and combined with the mean free path to yield satisfactory agreement with the experimental data. Of course, the correlation between MFP and r_s may also be only fortuitous.

The model also allows the crack growth parameters B and s in Eq. (18) to be related to derived crack tip plasticity and cyclic stress-strain parameters. The values computed from Eqs. (19) and (20) and shown in Table IV are remarkably close to those derived from experiment, and lend confidence to the model.

Another level of complexity in the growth of fatigue cracks, as yet not discussed here, may also be examined by the model presented. Direct observation of crack growth under conditions of high resolution has revealed that during the several loading cycles preceding crack extension,

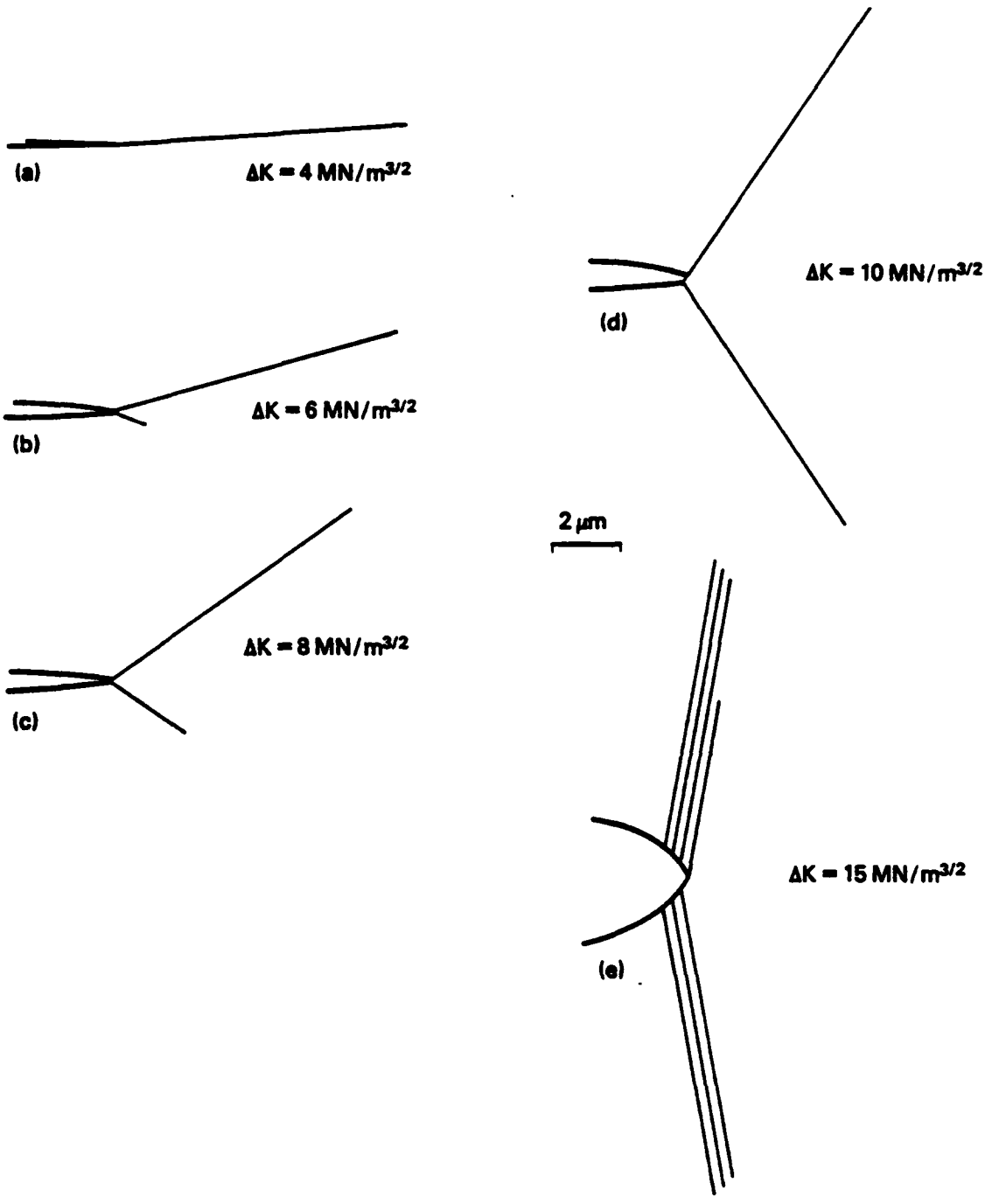

FIGURE 4. 7075-T651 FATIGUE CRACK GROWN IN VACUUM. The crack tip slip line configurations predicted by the model are drawn to scale. Note that the crack opening in (a) is too small to be accurately depicted, and in (e) the distance between slip lines is shown equal to $D_N b$. Values are taken from Table II.

TABLE V

SENSITIVITY OF THE SLIP LENGTH
TO THE CYCLIC STRESS-STRAIN CURVE

K_1 (MPa)	n	r_s (μm)
650	.0594	10.5
750	.0594	9.1
850	.0594	8.0
1000	.0594	6.8
775	.04	7.9
775	.05	8.4
775	.06	8.8
775	.07	9.3

TABLE VI

7075-T651 VACUUM
r_s = 5 μm

ΔK MN/m$^{3/2}$	4	6	8	10	12
θ	6.7	16.1	29.9	48.3	71.5
N(K)	1	1.7	2.5	3.6	5.3
D_N	584	628	661	688	711
$CTOD_x$	0.021	0.089	0.25	0.56	2.4
$CTOD_y$	0.17	0.054	0.034	0.055	0.02
Δa	0.17	0.31	0.43	0.49	0.35
Δa/ss	*	0.95	1.2	1.3	0.92

*Below measurement length.

the crack tip becomes increasingly blunt with each cycle [12]. Since crack tip strain and CTOD have been experimentally related by

$$\Delta\gamma_p = A\ C_o^{\ x} \tag{29}$$

the increase in CTOD is accompanied by an increase in strain at the crack tip [12]. These findings have been used to explain why a range of $\Delta\gamma_p$ and CTOD are determined for the same applied ΔK_{eff}; measurements of these factors were apparently made at various fractions of the number of cycles ΔN experienced by the crack tip prior to extension.

The model was derived considering only average behavior of the crack tip; however, the variation in CTOD and $\Delta\gamma_p$ which occurs at a fixed ΔK_{eff} can also be examined by considering the equations for $CTOD_x$, $D_N b$ and θ, Eqs. (4), (8) and (26). As the crack is cycled at a value of ΔK_{eff}, the angle of the slip lines is established by Eq. (26). Increases in CTOD occur by increases in either N(K) or $D_N b$, or both, according to Eq. (4), while increases in $\Delta\gamma_p$ will result in an increase in $D_N b$ proportional to $(\Delta\gamma_p)^{n'}$, according to Eq. (8), and assuming r_s is a fixed value. But n' is a small number, ~.06; therefore, changes in $\Delta\gamma_p$ of the magnitude observed result in small changes in $D_N b$, which means that nearly all the changes in $CTOD_x$ observed is due to a change in the number of slip lines N(K).

The odd number of slip lines computed by the model, Tables II, III and VI, may thus be interpreted as the result of using the average value of CTOD and $\Delta\gamma_p$. It is more realistic to think that N(K) must be a whole number, and that this would be achieved during the process of crack tip blunting which occurs prior to growth. As an example of this consider the model results in Table VI for ΔK = 6 MN/m$^{3/2}$ where N(K) = 1.7. At the beginning of the ΔN leading to crack advance, the slip line would be short, quickly lengthening to r_s in one or a few cycles. One more cycle would cause another slip line to form as $CTOD_x$ continued to increase, growing ultimately with more cycles to length r_s, just prior to crack advance. What started as one slip line ended as two as CTOD increased during ΔN. There were, however, only 1.7 slip lines required to produce the average CTOD at ΔK = 6 MN/m$^{3/2}$. For higher ΔK, the ΔN prior to crack advance is decreased (ultimately to 1 for $\Delta K \gtrsim 12$ MN/m$^{3/2}$); thus, there should be less variation in $CTOD_x$ and $\Delta\gamma_p$ since they will be nearly the same on each cycle. This seems to be consistent with observations [12].

This model is recognized as having limitations. Perhaps the most serious is that not all the factors associated with fatigue crack growth under constant cyclic loading are included in the model; e.g., it does not relate the existence of the threshold directly to metallurgical parameters, nor is the phenomenon of crack closure included. Through continued evolution, it may be possible to include such factors and to use theoretical determinations of CTOD and crack tip strain. The effects of environment may be partially included in the model through measured changes in CTOD and strain [12]. Environmental effects and the use of the model with other microstructures will be reported separately.

The model, as formulated, does not specifically include any effects of the crystallographic orientations of the grains through which the crack is growing. At this time, at least for aluminum alloys, there is insufficient information to include this factor. If the angle between the slip direction and the crack growth directions was known, it should be possible to test the model through use of the equations which have been derived.

e. Comparison With BCS Theory

The similarities between this model and the BCS theory for fatigue crack growth [24] are interesting: both models consider CTOD to be due to dislocations moving on slip planes, and that a number of cycles are required for a work hardening material to reach a condition of maximum crack tip displacement, which results in an increment of crack growth which is proportional to the crack tip displacement.

The present model differs from the BCS model in that the angle between the crack growth direction and the slip planes is variable (it is fixed in BCS at $\theta = 0$ or 45°), and the number of slip lines N(K) increases as ΔK increases (N(K) is fixed at 1 or 2 in BCS theory development). Stress is brought into the BCS theory directly through an applied stress on the cracked body and an average stress through the plastic zone, while the present model uses ΔK as a correlating parameter, with stress determined through the cyclic stress-strain curve and measured crack tip strain. The advantage of this latter approach is that crack length is not a factor in the model, and that stress enters through the macroscopic (engineering) parameter ΔK.

f. Summary and Conclusions

1. A crack tip slip line model has been hypothesized which is used in conjunction with crack tip deformation and growth data measured for an aluminum alloy to derive equations from which the length of the slip line and angle to the direction of crack growth may be computed.

2. The model when applied to 7075-T651 ingot alloy gives results which are compatible with the assumptions. The slip line length appears to be related to the mean free path between dispersoids.

3. The model introduces mixed mode crack tip opening displacement, which has been experimentally observed, and predicts that the Mode II component of CTOD will oscillate with decreasing ΔK, reaching a maximum at ΔK threshold.

g. References

[1] E. Hornbogen and K. H. Zum Gar, "Microstructure and Fatigue Crack Growth," Acta Met., 24, 581-592 (1976).

[2] J. Lindigkeit, A. Gysler, and G. Lutjering, "The Effect of Microstructure on the Fatigue Crack Propagation Behavior of an Al-Zn-Mg-Cu Alloy," Met. Trans. A, 12A, 1613 (1981).

[3] J. Lindigkeit, G. Terlinde, A. Gysler, and G. Lutjering, "The Effect of Grain Size on the Fatigue Crack Propagation Behavior of Age-Hardened Alloys in Inert and Corrosive Environment," Acta Met., 27, 1717-1726 (1979).

[4] G. Terlinde and G. Lutjering, "Influence of Grain Size and Age-Hardening on Dislocation Pile-Ups and Tensile Fracture for a Ti-Al Alloy," Met. Trans. A, 13A, 1283 (1982).

[5] S. B. Chakrabortty, "A Model Relating Low Cycle Fatigue Properties and Microstructure to Fatigue Crack Propagation Rates," Fatigue of Engng. Mater. and Struct., 2, 331-344 (1979).

[6] H. W. Liu and N. Ino, "A Mechanical Model for Fatigue Crack Propagation," Fracture 1969, Chapman and Hall Ltd, London, 1969, pp. 812-823.

[7] J. Lanteigne and J.-P. Bailon, "Theoretical Model for FCGR Near the Threshold," Met. Trans. A, 12A, 459 (1981).

[8] A. Saxena and S. D. Antolovich, "Low Cycle Fatigue, Fatigue Crack Propagation and Substructures in a Series of Polycrystalline Cu-Al Alloys," Met. Trans. A, 6A, 1809 (1975).

[9] S. Taira, K. Tanaka, and M. Hoshina, "Grain Size Effect on Crack Nucleation and Growth in Long-Life Fatigue of Low-Carbon Steel," ASTM STP 675, 135 (1979).

[10] P. Neumann, "New Experiments Concerning the Slip Processes at Propagating Fatigue Cracks-I," Acta Met., 22, 1155-1165 (1974).

[11] H. Vehoff and P. Neumann, "Crack Propagation and Cleavage Initiation in Fe-2.6% Si Single Crystals Under Controlled Plastic Crack Tip Opening Rate in Various Gaseous Environments," Acta Met., 28, 265-272 (1980).

[12] D. L. Davidson and J. Lankford, "The Effects of Water Vapor on Fatigue Crack Tip Mechanics in 7075-T651 Aluminum Alloy," Fatigue of Engng. Mater. and Struct., 6, 241-256 (1983).

[13] J. Lankford and D. L. Davidson, "Fatigue Crack Micromechanisms in Ingot and Powder Metallurgy 7XXX Aluminum Alloys in Air and Vacuum," Acta Met., 31, 1273-1284 (1983).

[14] J. S. Santner and M. E. Fine, "Fatigue Crack Propagation in Aluminum-Base Copper Alloys," Met. Trans., 7A, 583-593 (1976).

[15] J. P. Hirth and J. Lothe, "Theory of Dislocations," McGraw-Hill Publ. Co., New York, 1968, p. 704.

[16] D. L. Davidson and J. Lankford, "The Effect of Water Vapor on Fatigue Crack Tip Stress and Strain Range Distributions and the Energy Required for Crack Propagation in Low-Carbon Steel," Inter. Journ. of Fract., 17, 257-275 (1981).

[17] J. W. Hutchinson, "Plastic Stress and Strain Fields at a Crack Tip," J. Mech. Phys. of Solids, 16, 337-347 (1968).

[18] B. R. Kirby and C. J. Beevers, "Slow Fatigue Crack Growth and Threshold Behavior in Air and Vacuum of Commercial Aluminum Alloys," Fatigue of Engng. Mater. and Struct., 1, 203-215 (1979).

[19] D. L. Davidson and J. Lankford, "Mixed Mode Crack Opening in Fatigue," Materials Science and Engineering, 60, 225-229 (1983).

[20] E. A. Starke, private communication.

[21] S. H. Doerr, "A Comparison of Microstructure and Properties of Equivalent Strength Ingot Metallurgy and Powder Metallurgy 7XXX Aluminum Alloys," AFWAL-TR-81-4068, Materials Laboratory, Air Force Wright Aeronautical Laboratories, WPAFB, OH 45433, Aug. 1981.

[22] J. W. Martin, "Micromechanisms in Particle-Hardened Alloys," Cambridge University Press, 1980, Ch. 1.

[23] P. E. Bretz, A. K. Vasudevan, R. J. Bucci and R. C. Malcolm, "Effects of Microstructure on 7XXX Aluminum Alloy Fatigue Crack Growth Behavior Down to Near-Threshold Rates," Final Report to Naval Air Systems Command Contract N00019-79-C-0258 by Aluminum Company of America, October 1981, p. 51.

[24] J. Weertman, "Theory of Fatigue Crack Growth Based on BCS Crack Theory with Work Hardening," Inter. J. Fracture, 9, 125-130 (1973).

B. Task 2. Fracture Mechanisms in Single Crystal Nickel-Base Superalloys

1. Scope

The improved creep-rupture properties of single crystal nickel-base superalloys compared to columnar-grained and conventionally cast blade materials make them attractive for the next generation of turbine blades in advanced military gas turbine engines. In contrast to conventionally cast alloys, the mechanical properties of the single crystal superalloys are highly anisotropic. The effect of the anisotropy on the mechanisms of creep in this class of alloys has been extensively studied over the temperature range 760-1000°C. Although fatigue crack initiation has been characterized for single crystal superalloys with an [001] tensile axis orientation, very little is known about crack growth in these materials. In particular, the effects of the relative alignment of the crystallographic orientation with respect to the applied stress state have yet to be determined.

The current program is aimed at identifying and modeling the key factors controlling subcritical crack growth and unstable fracture in single crystal nickel-base superalloys. The experiments are concentrating on the influence of the angles between the loading axis and the crystallographic axes of the material for both unidirectional and multiaxial loading. In addition, experiments are planned in both the low and intermediate temperature range where hetereogeneous, planar slip is predominant and in the higher temperature regime where homogeneous, wavy slip prevails. γ' size and distribution will also be used as a variable to effect a change in slip character.

2. Current Status

The basic concepts of anisotropic elasticity have been used to develop a fracture mechanics approach to crack tip deformation and crack growth phenomena in single crystals. This approach was subsequently used to design an appropriate test matrix for the single crystal orientations of interest. Severe delays were encountered in material delivery due to difficulties encountered by the casting vendor during processing. Thus, the testing phase could not begin before the eleventh month of the twelve-month reporting period. The efforts to date will be discussed as follows: 1) a review of anisotropic fracture mechanics and crack tip stress fields; 2) a description of the material and experimental procedures; 3) presentation of initial crack growth results in notched, multiaxially loaded tubes; and 4) a discussion of the slip character in ordered $L1_2$ crystal structures.

a. Anisotropic Fracture Mechanics

The basic descriptions of plane anisotropic elasticity have been described by Lekhnitski [1] and Sih and Liebowitz [2]. A complex analytic function is defined such that

$$\frac{d\Phi_i(z)}{dz} \equiv \Phi_i'(z) \equiv \psi_i(z) \tag{1}$$

Then the three independent stresses become

$$\begin{aligned} \sigma_{xx} &= 2\ \mathrm{Re}\ [\mu_1^2\psi_1(z_1) + \mu_2^2\psi_2(z_2)] \\ \sigma_{yy} &= 2\ \mathrm{Re}\ [\psi_1(z_1) + \psi_2(z_2)] \\ \tau_{xy} &= -2\ \mathrm{Re}\ [\mu_1\psi_1(z_1) + \mu_2\psi_2(z_2)] \end{aligned} \tag{2}$$

where the μ_i are roots of a characteristic equation

$$a_{11}\mu^4 - 2a_{16}\mu^3 + (2a_{12} + a_{66})\mu^2 - 2a_{26}\mu + a_{22} = 0 \tag{3}$$

with the a_{ij} being the elastic compliances. The solution of the stress field involves the determination of $\Phi_1(z_1)$ and $\Phi_2(z_2)$ where:

$$z_j = x_j + iy_j \tag{4}$$

The procedure for the anti-plane problem is similar but only one function needs to be found, z_3.

Due to the crystallographic nature of the cracking expected at low to intermediate temperatures, a crack tip stress field which allows for the operation of all three crack opening modes is required. The general plane strain anisotropic crack tip field solution for an orthotropic plate is given by [2,3]:

$$\begin{aligned} \sigma_{xx} &= \frac{K_I}{\sqrt{2\pi r}}\ \mathrm{Re}\left[\frac{\mu_1\,\mu_2}{\mu_1-\mu_2}\left(\frac{\mu_2}{d_2} - \frac{\mu_1}{d_1}\right)\right] + \frac{K_{II}}{\sqrt{2\pi r}}\ \mathrm{Re}\left[\frac{1}{\mu_1-\mu_2}\left(\frac{\mu_2^2}{d_2} - \frac{\mu_1^2}{d_1}\right)\right] \\ \sigma_{yy} &= \frac{K_I}{\sqrt{2\pi r}}\ \mathrm{Re}\left[\frac{\mu_1\,\mu_2}{\mu_1-\mu_2}\left(\frac{1}{d_1} - \frac{1}{d_2}\right)\right] + \frac{K_{II}}{\sqrt{2\pi r}}\ \mathrm{Re}\left[\frac{1}{\mu_1-\mu_2}\left(\frac{\mu_1}{d_1} - \frac{\mu_2}{d_2}\right)\right] \\ \sigma_{zz} &= \nu(\sigma_{xx} + \sigma_{yy}) \\ \tau_{xy} &= \frac{K_I}{\sqrt{2\pi r}}\ \mathrm{Re}\left[\frac{1}{\mu_1-\mu_2}\left(\frac{\mu_1}{d_1} - \frac{\mu_2}{d_2}\right)\right] + \frac{K_{II}}{\sqrt{2\pi r}}\ \mathrm{Re}\left[\frac{1}{\mu_1-\mu_2}\left(\frac{1}{d_2} - \frac{1}{d_1}\right)\right] \\ \tau_{xz} &= \frac{-K_{III}}{\sqrt{2\pi r}}\ \mathrm{Re}\left[\frac{\mu_3}{d_3}\right] \\ \tau_{yz} &= \frac{K_{III}}{\sqrt{2\pi r}}\ \mathrm{Re}\left[\frac{1}{d_3}\right] \end{aligned} \tag{5}$$

where: K_j = stress intensity factor for Mode j.

$d_j = (\cos\theta + j;\ \sin\theta)^{1/2}$.

r = distance from the crack tip to the point of interest.

θ = angle between the crack plane and the point of interest.

Lekhnitski [1] recognized that once the μ_j are known in a plane of elastic symmetry, μ_1 and μ_2 can be rotated in the plane through an angle ϕ by:

$$\mu_1' = \frac{\mu_1 \cos\phi - \sin\phi}{\cos\phi + \mu_1 \sin\phi} \qquad \mu_2' = \frac{\mu_2 \cos\phi - \sin\phi}{\cos\phi + \mu_2 \sin\phi}$$

$$\bar{\mu}_1' = \frac{\bar{\mu}_1 \cos\phi - \sin\phi}{\cos\phi + \bar{\mu}_1 \sin\phi} \qquad \bar{\mu}_2' = \frac{\bar{\mu}_2 \cos\phi - \sin\phi}{\cos\phi + \bar{\mu}_2 \sin\phi} \tag{6}$$

Thus, for a plate of material with its cube axes aligned with the axes of the plate, a_{16} and a_{26} are equal to zero and the characteristic equation becomes:

$$a_{11}\mu^4 + (2a_{12} + a_{66})\mu^2 + a_{22} = 0 \tag{7}$$

This is a simple quadratic in μ^2. The μ_j for all orientations of specimens lying within the plane of the plate can be simply solved by combining Equations (6) and (7).

In addition, Rau and Cook [4] have pointed out that, as long as one can assume an infinite body and the stresses on the crack are zero or self-equilibrating, the stress intensity factors for the various modes are identical to their isotropic counterparts. It should be noted here that although the crack tip stress intensity factors are not influenced by anisotropy the stress and, therefore, deformation fields are responsive to the degree of anisotropy (see Equation (5)).

As a relevant example, consider the geometry of a thin-walled tube containing a crack shown in Figure 1. For our purposes, an alternating σ_{yy} and σ_{xy} stress combination will be applied. The direction cosines between the tube coordinates (xyz) and the crack coordinates (x'y'z') are given in Table I.

Then:

$$\begin{aligned}
\Delta\sigma_{y'y'} &= \Delta\sigma_{yy} m_2^2 + 2\Delta\tau_{xy} \ell_2 m_2 \\
\Delta\tau_{x'y'} &= \Delta\sigma_{yy} m_1 m_2 + \Delta\tau_{xy}(\ell_1 m_2 + m_1 \ell_2) \\
\Delta\tau_{y'z'} &= \Delta\sigma_{yy} m_2 m_3 + \Delta\tau_{xy}(m_2 \ell_3 + \ell_2 m_3)
\end{aligned} \tag{8}$$

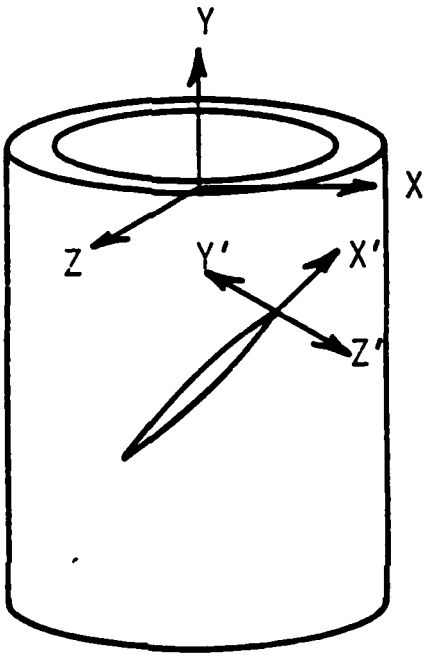

FIGURE 1. CRACKED THIN-WALL TUBE GEOMETRY USED FOR EXAMPLE STRESS INTENSITY FACTOR CALCULATION.

and:

$$\Delta K_I = \beta \, \Delta\sigma_{y'y'} \sqrt{\pi a}$$

$$\Delta K_{II} = \beta \, \Delta\tau_{x'y'} \sqrt{\pi a}$$

$$\Delta K_{III} = \beta \, \Delta\tau_{y'z'} \sqrt{\pi a}$$

where β is a correction factor for curvature in tubular specimens, Figure 2 [5]. Although most of the crystallographic cracking in the tubular specimens would not be expected to lie either along or perpendicular to the axis of the tubes, it is felt that a good estimate of β for other angles can be derived from the data in Figure 2. This is particularly true, since the maximum λ reached prior to failure to date has been approximately 1.4.

TABLE I

DIRECTION COSINES BETWEEN
x y z and x′ y′ z′

	x	y	z
x′	l_1	m_1	n_1
y′	l_2	m_2	n_2
z′	l_3	m_3	n_3

b. Material and Experimental Procedure

The material chosen for this study was a modified Mar-M-200 composition consisting of Ni-9Cr-10Co-12.5W-1Nb-4.7Al-1.7Ti-<50 ppm C. The Al and Ti contents are slightly lower than those found in commercial Mar-M-200 to avoid the formation of eutectic γ' pools. C is also kept to a minimum to prevent the formation of carbides. Thus, the resultant microstructure is very clean with only γ' precipitates in a matrix of γ. Both plate and rod single crystal material were solutionized at 2250°F for four hours and subsequently aged at 1600°F for 32 hours. This heat treatment yielded a uniform distribution of cuboidal γ' precipitates approximately 0.2 μm on edge.

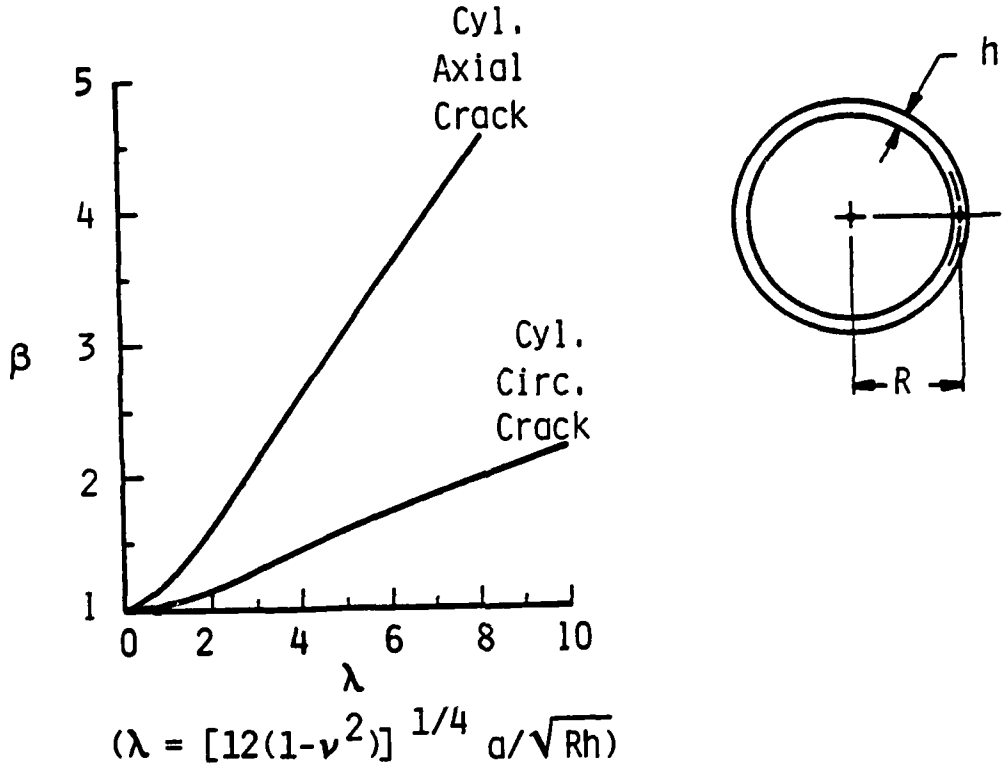

FIGURE 2. β, THE CURVATURE CORRECTION FACTOR, AS A FUNCTION OF CRACK LENGTH NORMALIZED TO SPECIMEN GEOMETRY.

Single crystal rods were machined into tubular specimens while the plate single crystal material was machined into standard compact tension specimens. A photograph of typical specimens along with a small tensile specimen is shown in Figure 3. A catalog of specimen orientations for the tubes and compact tension specimens is given in Tables II and III, respectively. Also included in Table II is the orientation of the center of an 0.040" long through-thickness notch placed perpendicular to the axis of the cube axis tubular specimens. The test schedule for the three specimens with their notches centered on [001] includes tension-torsion fatigue in one each of the following three conditions: 1) $\Delta\sigma = 2\Delta\tau$; 2) $\Delta\sigma = \Delta\tau$; and 3) $\Delta\tau = 2\Delta\sigma$. The tests are run under load control with an increasing stress intensity range due only to crack growth. The absolute levels of tension and shear are being adjusted to give an initial effective stress intensity range of 14 ksi$\sqrt{\text{in.}}$ for all three conditions. The tension is applied with an R ratio of 0.1 while the torsion is fully reversed. The two loads are applied in phase with the frequency of the tension twice that of the torsion. Initial tests are being conducted at room temperature.

Testing under conditions 1) and 3) have been completed and will be described in the next section. The specimen for condition 2) is currently being run. Based on the results of these three tests the fourth cube axis specimen, with its notch centered on [011] will be fatigued under one of the three conditions listed above to provide data on the effect of orientation as well as applied stress state on multiaxial crack growth. Similar matrices are planned for the remaining specimens. During the test, crack length and slip orientations are being documented by making periodic replicas of the crack tip regions on both sides of the notch.

All compact tension specimens will be run with the notch cut perpendicular to the stress axis. Electron and optical microscopy are being used to characterize all subcritical crack growth fracture surfaces and deformation modes. Deformation patterns will be compared to those expected from the resolution of the calculated crack tip stress fields onto possible slip planes.

c. Initial Multiaxial Fatigue Results

The crack growth experiments using notched tubular specimens with a cube axis and a cube direction perpendicular to the center of the notch have been completed for conditions 1 and 3. A plot of real crack length, a, versus number of cycles is given in Figure 4 for both of these tests. Two sets of data are presented for each condition due to the presence of cracks on both sides of the notch. As can be seen from the data, a significant difference in crack growth rate is brought about by changing the ratio of normal to shear stresses. Although both tests were begun with identical values of effective stress intensity range and data collection started at a crack length of 0.005 inches, the cracks in the specimen which was loaded to a value of tension twice that for shear grew considerably faster than those in the specimen which was loaded to value of tension half that for shear. Although this implies a pronounced effect of the individual stress components on crack growth rate at a given

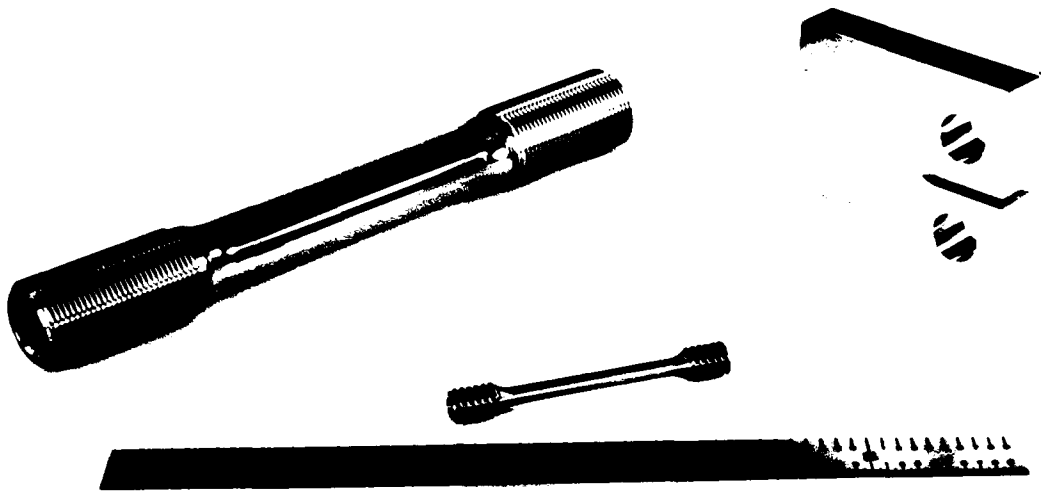

FIGURE 3. TYPICAL SINGLE CRYSTAL SPECIMENS USED IN THIS STUDY. Clockwise from upper left: 1) notched tubular multiaxial specimen; 2) compact tension specimen; 3) tensile specimen.

TABLE II

TENSION-TORSION FATIGUE SPECIMENS

No. of Specimens	Axis Orientation	Direction Perpendicular to Center of Notch
3	<110>	-
3	<001>	<001>; <001>; <110>
2	6-8° off <001>	-
1 (w/high angle grain boundary)	<001>	<001>
1 (w/high angle grain boundary)	22° off <001>	-

TABLE III

COMPACT TENSION SPECIMENS

No. of Specimens	Notch Plane	Notch Direction	Notch Front
4	(010)	<100>	<001>
3	(110)	<1$\bar{1}$0>	<001>
2	(111)	<2$\bar{1}\bar{1}$>	<0$\bar{1}$1>
1	(230)	<3$\bar{2}$0>	<001>
1	(120)	<2$\bar{1}$0>	<001>
1	(150)	<5$\bar{1}$0>	<001>
1	(130)	<3$\bar{1}$0>	<001>

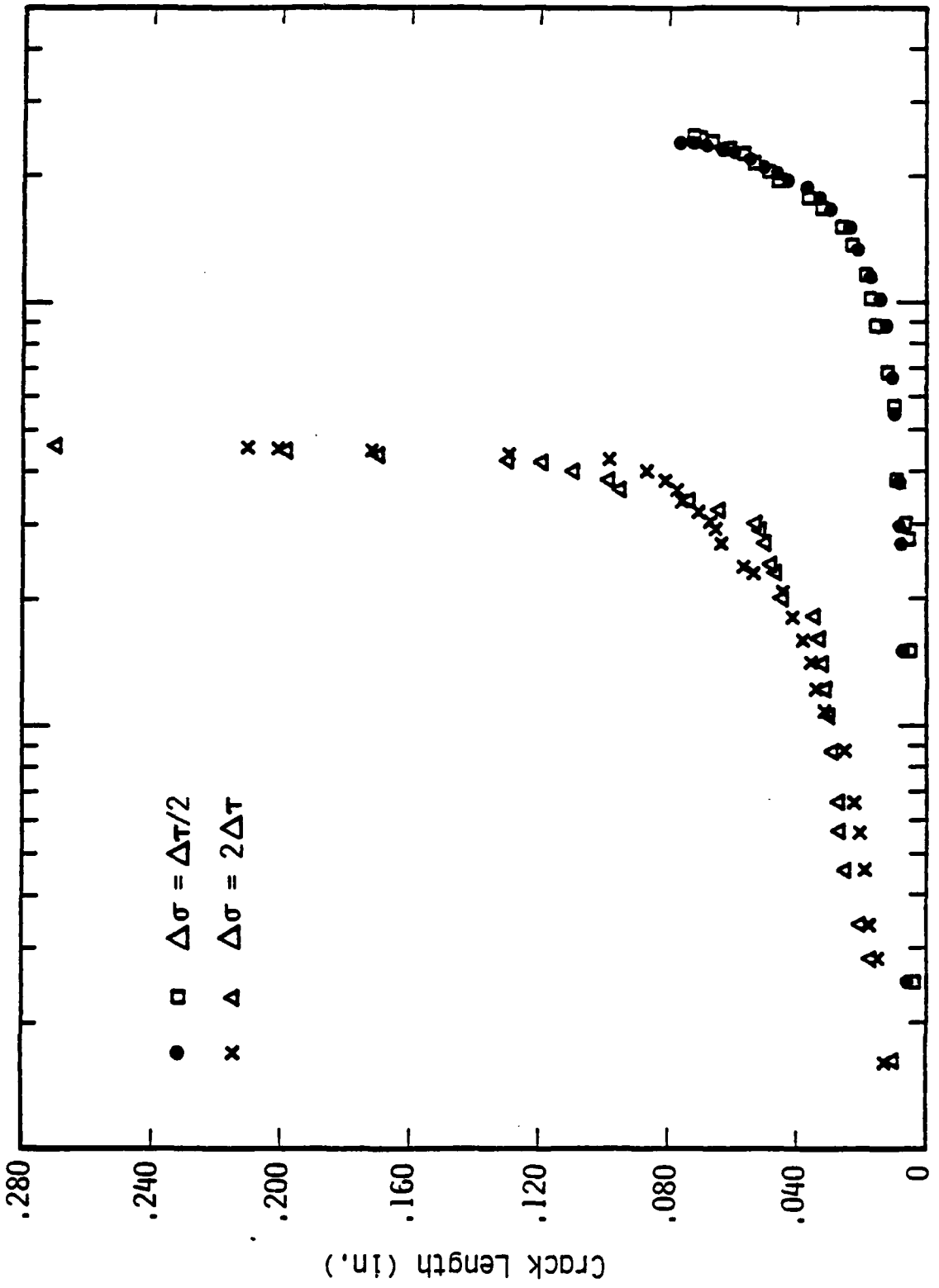

FIGURE 4. CRACK LENGTH VERSUS THE NUMBER OF CYCLES FOR TWO APPLIED MULTIAXIAL STRESS STATES AT AN INITIAL ΔK_{eff} OF 14 ksi$\sqrt{in}$.

effective stress intensity range, some other factors could possibly contribute to the observed difference. These include an increased amount of surface roughness induced crack tip closure as the ratio of shear to tension is increased and an initially slow growth rate due to multiple cracking at the notch tips prior to the establishment of dominant cracks on either side of the notch.

The latter effect is presumably small because multiple cracking was observed in both specimens and the marked difference in crack growth rate was retained when dominant cracks were established on both sides of the notch. The influence of roughness induced closure will have to be estimated from fractographic observations. Detailed fractography is currently being conducted along with the determination of active slip planes. However, initial results do indicate that the subcritical crack growth mode is cyclic cleavage along (111) slip planes, as would be expected from results on identical single crystal material [6].

d. Influence of Slip Character on Crack Growth

It has been noted that above ≈1400°F the slip character in this modified Mar-M-200 alloy changes from planar to wavy. Takeuchi and Kuramoto [7] and Pope and co-workers [8-10] have shown a similar transition in single phase materials based on the same crystallography as the $Ni_3(Al, Ti, Nb)$ γ' phase present in this alloy. They showed that the transition was due to the onset of macroscopic slip on the cube plane and that the transition temperature was also strongly orientation dependent. A similar transition in slip character was recently reported by Chen and McEvily [11]. In that case, however, the transition occurred at room temperature in samples compressed along a [111] axis as the size of the cuboidal γ' particles increased from 3.9×10^{-6} inches to 1.8×10^{-5} inches. They gave evidence that cube slip was responsible for the transition which they observed as well. Although the occurrence of cube slip only in specimens with the [111] axis would tend to agree with the previous results and the fact that the ratio of the Schmid factors for cube and octahedral slip is highest for this orientation [7-10], cube slip normally requires a large thermal activation and would not be expected to occur at room temperature.

Chen and McEvily [11] have ascribed their observations to the relative size of the γ' particles compared to the jog spacing along the leading dislocation of a pair of dislocation about to cut through an ordered γ' particle. They argue that, for small γ' particle sizes, the thermally activated jog density along the leading dislocation is such that the jogs are more widely spaced than the particle size. From the model of Takeuchi and Kuramoto, properly oriented jogs are required for cross slip onto the cube plane to occur at temperatures below the transition temperature for macroscopic cube slip. Thus, an increase in γ' particle size would be expected to increase the number of jogs interacting with a given γ' particle in an analogous way to increasing the jog density by increasing the temperature.

Whether or not this explanation is valid, the observed relationship between γ' size and slip character does present the possibility of studying the effect of slip character on crack growth at room temperature. Thus, selected material is being resolutionized and aged just below the γ' solvus to generate material with a uniform distribution of relatively large cuboidal γ' particles. Cracks will then be grown through specimens with this microstructure which have been oriented to promote cube slip around the starting notch. Their behavior will then be compared to results in materials with fine γ' particles that show only octahedral slip.

e. References

[1] S. G. Lekhnitski, Anisotropic Plates, American Iron and Steel Institute, New York, New York, 1956.

[2] G. C. Sih and H. Liebowitz, in Fracture: An Advanced Treatise, Vol. 2, H. Liebowitz, ed., Academic Press, New York, New York, 1968, p. 67.

[3] G. P. Cherepanov, Mechanics of Brittle Fracture, McGraw-Hill, New York, New York, 1979.

[4] T. S. Cook and C. A. Rau, Jr., in Prospects of Fracture Mechanics, G. C. Sih, H. C. Van Elst and D. Broek, eds., Noordhoff International Publishing, Leyden, The Netherlands, 1974, p. 509.

[5] F. Erdogan and M. Ratwani, Nuclear Engineering and Design, 20, 265 (1972).

[6] G. R. Leverant and M. Gell, Metallurgical Transactions A, 6A, 367 (1975).

[7] S. Takeuchi and E. Kuramoto, Acta Metallurgica, 21, 415 (1973).

[8] S. J. Liang and D. P. Pope, Acta Metallurgica, 25, 485 (1977).

[9] C. Lall, S. Chin and D. P. Pope, Metallurgical Transactions, 10A, 1204 (1979).

[10] V. Paidar, D. P. Pope and M. Yamaguchi, Scripta Metallurgica, 15, 1029 (1981).

[11] O. Y. Chen and A. J. McEvily, "The Effect of Gamma Prime Size on the Deformation Characteristics of Single Crystal Nickel-Base Superalloy Mar-M-200 Along Various Crystallographic Orientations," presented at the 113th Annual AIME Meeting, Los Angeles, CA, February 26-March 1, 1984.

III. PUBLICATIONS (AFOSR SPONSORSHIP)

1. "Experimental Mechanics of Fatigue Crack Growth: The Effect of Crack Size," D. L. Davidson and J. Lankford, Proceedings Eshelby Memorial Symposium, Cambridge University Press, 1984 (in press).

2. "Experimental Mechanics and Modeling of Fatigue Crack Growth," D. L. Davidson, Proceedings of Modelling Problems in Crack Tip Mechanics, University of Waterloo Press, 1984 (in press).

3. "A Model for Fatigue Crack Advance Based on Crack Tip Metallurgical and Mechanics Parameters," D. L. Davidson, Acta Metallurgica, March, 1984 (in press).

IV. PROGRAM PERSONNEL

Name	Title	
Dr. James Lankford	Staff Scientist	Co-principal Investigators
Dr. David L. Davidson	Institute Scientist	
Dr. Gerald R. Leverant	Assistant Director, Materials Sciences	
Mr. John E. Hack	Senior Research Metallurgist	
Dr. K. S. Chan	Research Engineer	
Mr. Ronald McInnis	Senior Technician	
Mr. John Campbell	Senior Technician	
Mr. Harold Saldana	Senior Technician	

V. INTERACTIONS - 1983

A. Task 1. Influence of Metallurgical Structure Upon Crack Tip Micromechanics

1. Paper - Fall AIME Meeting, Philadelphia, "A Model for Fatigue Crack Growth Combining Measured Crack Tip Parameters with Geometric and Microstructural Considerations," 4 Oct.

2. Symposium - Organization and Chairmen of Sessions, Fall AIME Meeting, Philadelphia, "Fatigue Crack Growth Threshold Concepts," 5 sessions, 3-5 Oct.

3. Seminar - Alcoa, "Fatigue Crack Growth in Aluminum Alloys: Experimental Mechanics and Modeling," 7 Nov.

4. Seminar - WPAFB, "Fatigue Crack Growth in Titanium Alloys," 8 Nov.

5. Telephone Contacts with Sharon Langenbeck at Lockheed and Greg Hildebrand at Alcoa concerning high temperature aluminum alloys of the Al-Fe-Ce composition which we have begun to test at temperature.

B. Task 2. Fracture Mechanisms in Single Crystal Nickel-Base Superalloys

1. A dialogue has been maintained with Dr. A. F. Giamei, United Technologies Research Center. He is planning to visit SwRI during the first half of 1984.

2. A paper entitled, "Considerations for the Multiaxial Fatigue of Nickel-Base Superalloy Single Crystals," by J. E. Hack, K. S. Chan and G. R. Leverant, was presented at the 113th Annual AIME meeting in Los Angeles, CA, February 27, 1984.

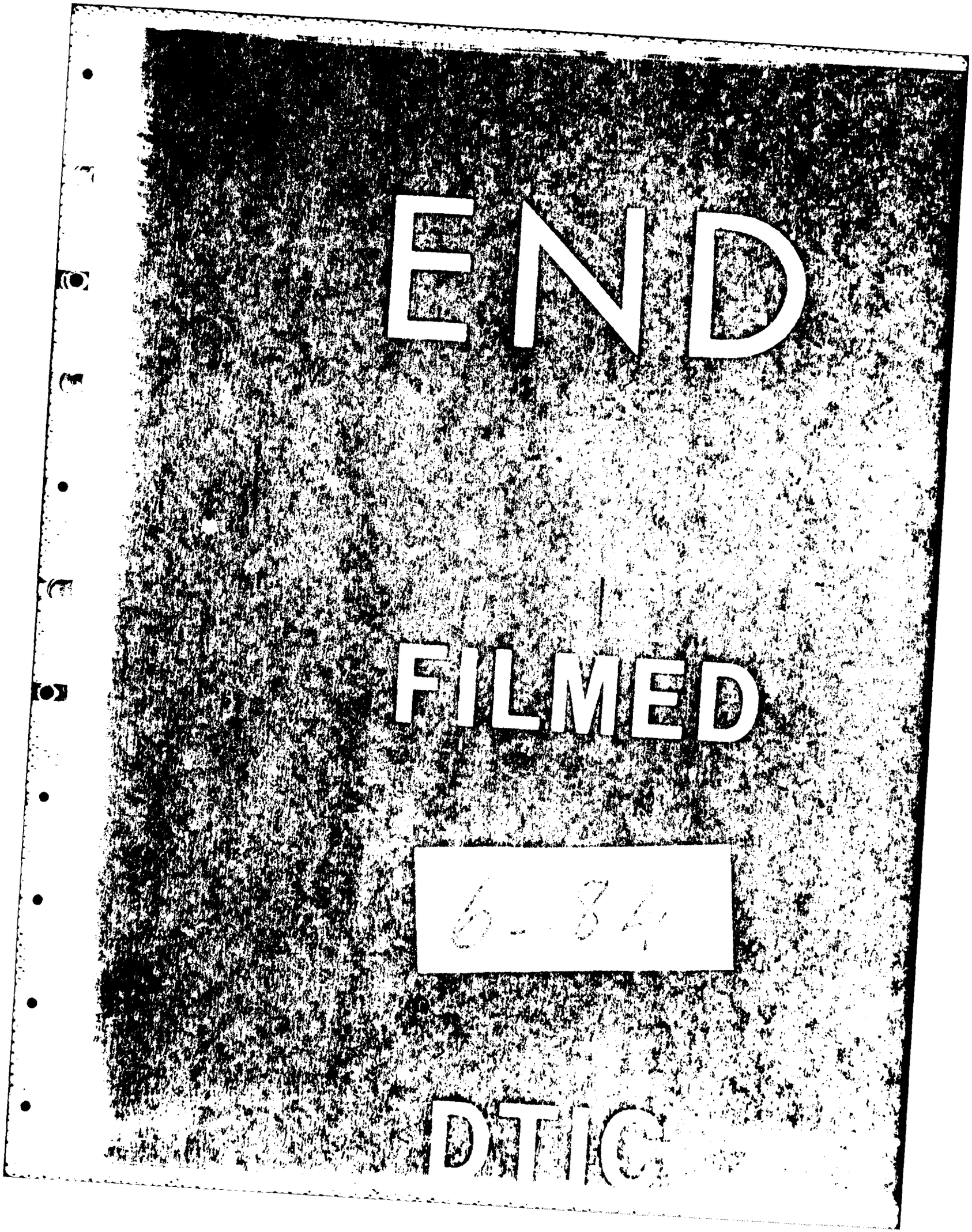
END
FILMED
6-84
DTIC